IGC Newsletter

ISSN 0972-5741 Volume 133, Issue 3, July 2022

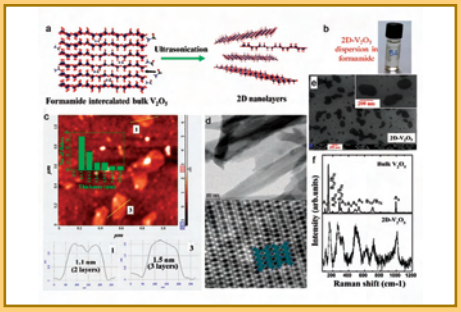

Director's Message

Dear Readers,

It gives me immense pleasure to share with you the Foundation Day celebrations of IGCAR on 30th April 2022. I am deeply grateful to all the seniors who graced the event. I dedicate this event to all the colleagues present and past of this particular Centre. Chairman, AEC and Secretary Department of Atomic Energy, Shri K.N. Vyas conveyed his best wishes through a video message.

IGCAR has established an Integrated Radiation Monitoring Facility (IRMF) at Anupuram to serve the radiation monitoring needs of Kalpakkam DAE complex and the public during radiological emergencies. This facility has in-vivo & in-vitro monitoring labs and a decontamination center. IRMF is established outside the DAE Complex to meet the regulatory requirements of AERB & NDMA. Shri. G. Nageswara Rao, Chairman, inaugurated the facility on the same day.

This year 2022, is unique because it is the 51st year since the inception of IGCAR erstwhile Reactor Research Centre which was founded on 30th April 1971. In 1968 a decision was taken to initiate the fast reactor programme by the Reactor Engineering Division, BARC. In 1969, CEA France and DAE signed an agreement to set up a Fast Breeder Reactor. Dr. Vikram Sarabhai is this programme's architect and has emphasized the closed fuel cycle concept.

In 1972, we had the ground breaking ceremony for the FBTR and many milestones culminating during the first criticality of FBTR in 1985.

FBTR has attained its rated capacity of 40 MW Thermal on the 7th March 2022. It has been successfully synchronized to the grid and has been operating smoothly for over 35 days. FBTR has generated around 2.27 million units of electricity as on date, earning a revenue of more than 3.5 Crores and it has been a cradle for human resource development.

Continue ...

FBTR today has a unique combination of Uranium Carbide and Plutonium Carbide fuel, the first of its kind in the world, thanks to the designers at the Bhabha Atomic Research Centre. The Nuclear Fuel Complex had ensured the delivery of the sub-assemblies.

FBTR is a forerunner of Atmanirbhar Bharat. When FBTR was conceived, a team from France and India visited the Indian industries and decided that the Indian industries were capable of manufacturing most of the components. 80% of the components were manufactured in India. FBTR is a classic example of Atmanirbhar Bharat.

We have also gone into irradiation of Yttria to produce Strontium-89 which would serve as palliative care for cancer therapy. FBTR is a test bed for irradiation of different materials and fuels. Along with FBTR, in 1972, the Fuel Reprocessing Development Laboratory (FRDL) was started and commissioned in 1976. Subsequently, in 1996, COmpact Reprocessing facility for Advanced fuels in Lead cells (CORAL) was started. Today the 62nd campaign is in progress. With the experience gained in CORAL, we have begun Demonstration Fuel Reprocessing Plant (DFRP). After the cold commissioning of DFRP by following all the regulatory requirements, we will start the first chopping of the Uranium Oxide Fuel pins. A team steered by Dr. Ananthasivam will ensure DFRP would enter into hot commissioning and this would be a milestone activity at IGCAR this year. I appreciate the efforts of the editorial committee and the author's contributions to the Newsletter.

JaiHind

(B. Venkatraman)

Director, IGCAR

Editor's Desk

Dear Reader
Greetings

It is my pleasant privilege to forward the latest issue of IGC Newsletter (Volume 133, July 2022, Issue 3). I thank my team for their timely inputs, cooperation, and support in bringing out this issue.

The digital copy is published at http://www.igcar.gov.in and is available on the intranet at http://vaigai as a flip copy.

Director's message includes excerpts from Foundation Day speech.

In this issue, we have two technical articles, the article by the young officer is entitled "Characterization of High-Temperature Fracture Behavior of Grade 91 steel" by Mr. B. Shashank Dutt from Materials Development and Technology Division, MMG, IGCAR. The young researcher is Ms. P. R. Reshma from Surface & Nanoscience Division, MSG, IGCAR. Her article is on "2D-V2O5 Nanosheets for Photocatalytic and Advanced Energy Storage Applications".

I am happy to share the awards and honors earned by our colleagues from April to June 2022. Foundation Day, the inauguration of the Integrated Radiation Monitoring Facility at Anupuram, and the workshop on IPR are a few of the events covered in this issue.

In every issue, a page is dedicated to Biodiversity at DAE Complex Kalpakkam. In this issue, Little Grebes, a water bird who visits every year and stays for six months with us is seen posing elegantly.

The Editorial Committee would like to thank all the contributors. We look forward to receiving constructive suggestions from readers towards improving the IGC Newsletter content.

We express our deepest gratitude to Director IGCAR for his keen interest and guidance.

With best wishes and regards

S. Rajeswari

Chairman, Editorial Committee, IGC Newsletter and

Head, Scientific Information Resource Division, IGCAR

Young Officer's Forum

Mr. B. Shashank Dutt is working as a Scientific Officer 'E' at the Materials Development and Technology Division, Indira Gandhi Centre for Atomic Research. He acquired B.Tech (Metallurgical Engineering) from NIT Rourkela and M.S (Research) (Metallurgical Engineering) from IIT Madras, Chennai, before joining IGCAR. His research interests include experimental fracture mechanics studies of various ferritic and austenitic steels, including base and welds. He has authored/co-authored 14 peer reviewed research articles in international journals.

Characterization of High Temperature Fracture Behavior of Grade 91 steel

Modified 9Cr-1Mo (or Grade 91 steel) is the material for steam generator (SG) components of Indian fast breeder reactor and these components are subjected to operating temperatures between 370 and 550 °C. The fracture toughness (J1c) and J-R curves at these operating temperatures are required for assessing the structural integrity of SG components. The extensive characterization of tensile properties of Grade 91 steels indicated that the metallurgical phenomenon called dynamic strain aging (DSA) influences these properties in this operating temperature range. In a similar manner, fracture behavior can be influenced by DSA, since the fracture behavior is a function of strength and ductility. Thus, this investigation has been undertaken to characterize fracture behavior of this steel in the temperature range 300-550 °C.

The Grade 91 steel was subjected to tensile testing at test temperatures 300, 350, 400, 450, 500 and 550 °C and as per ASTM E8 standard. The results of yield strength and tensile strength were presented in Figure 1(a) and Figure 1(b) respectively. The yield strength was observed to decrease with test temperatures. On the other hand, a ductility minimum was observed in the temperature range 400-450 °C, as shown in Figure 1(b). Peak in strain hardening exponent values can be revealed in Figure 2. All these are indicative of classical occurrence of dynamic strain aging (DSA). The fracture behavior in the form of J-R curves were established, fracture toughness (J1c) and tearing modulus values were determined for

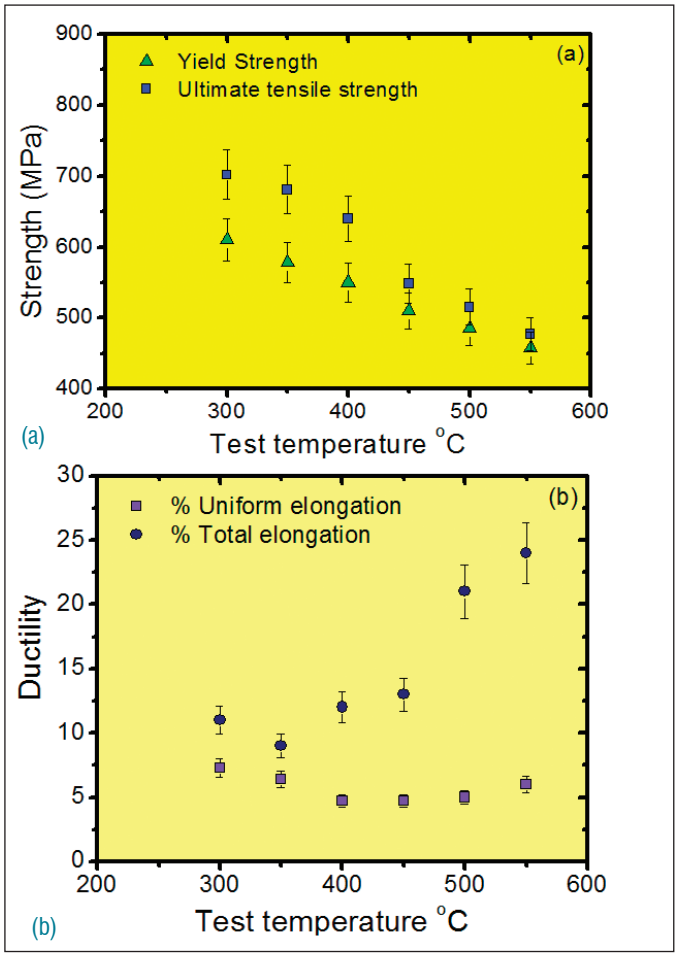

Figure 1 (a-b) : Tensile properties of the steel (a) Yield strength and tensile strength (b) ductility

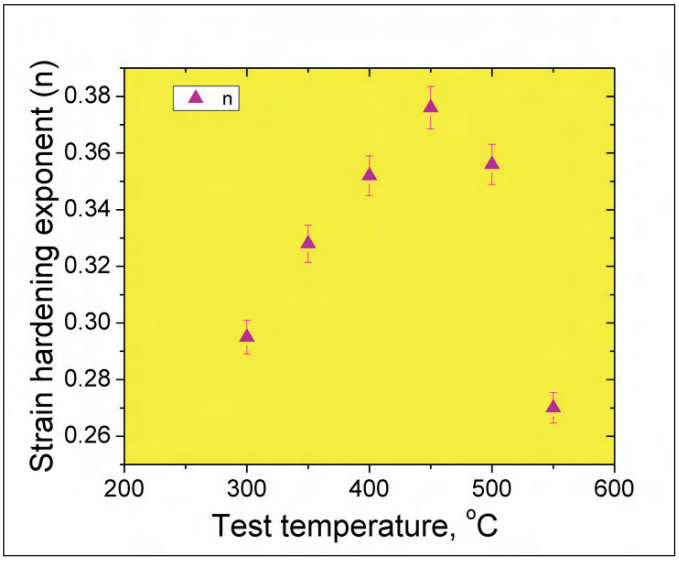

Figure 2 : Strain hardening exponent values

the above mentioned test temperatures at different loading (quasi-static) rates as per ASTM E1820. Compact tension (CT) specimens of 20 mm thickness were used for fracture testing. After fracture testing CT specimens were broken and stretch zone width (SZW) measurements carried out in SEM (Scanning Electron Microscope) in order to further understand the crack growth behavior.

The J-R curves obtained at different test temperatures are shown in Figure 3a. The initiation fracture resistance (J1c) values at various temperatures and different loading rates are shown in Figure 3b. Minimum in fracture toughness values were observed in the temperature range 350-450 °C and for all loading conditions. These observations are in line with minima in ductility as shown in Figure 1(b) in the similar temperature range. No significant changes in the tearing modulus values (Figure 4a) were observed in the temperature range 350-450 °C, though above this temperature a significant increase was observed for all loading rates. The average SZW values (plotted in Figure 4b) are found to be in the range 0.13 - 0.21 mm, for the above mentioned temperatures. Also, no significant changes in SZW values (Figure 4b) were observed in the temperature range 300-450 °C. A similar tends in the fracture toughness and ductility dip could be attributed to the DSA.

In order to establish the crack growth mechanism in the DSA regime, activation energy has been estimated. A generic formula for various steels the activation energy during DSA is determined by the equation (1):

$$\dot{\varepsilon} = A\exp(-(Q/RT)) \quad (1)$$

Where the dependence of strain rate (έ) on Temperatures (T, K) are considered and Q is the action energy. To understand the mechanism for DSA under different loading rates, activation energy was calculated by plotting the effective strain rates at crack tip (έ) (from the loading rates) with inverse of temperatures (1000/T, T in K). The crack tip strain rate was calculated based on equation (2):

$$\dot{\varepsilon} = (1.455)^n \frac{\Delta_L}{a\, h_3(a/w, n)} \quad (2)$$

Where the equivalent crack tip strain rate (έ) was calculated from the loading rates (ΔL), crack length (a), specimen width (w) and strain hardening exponent (n). The crack tip strain rate (equation

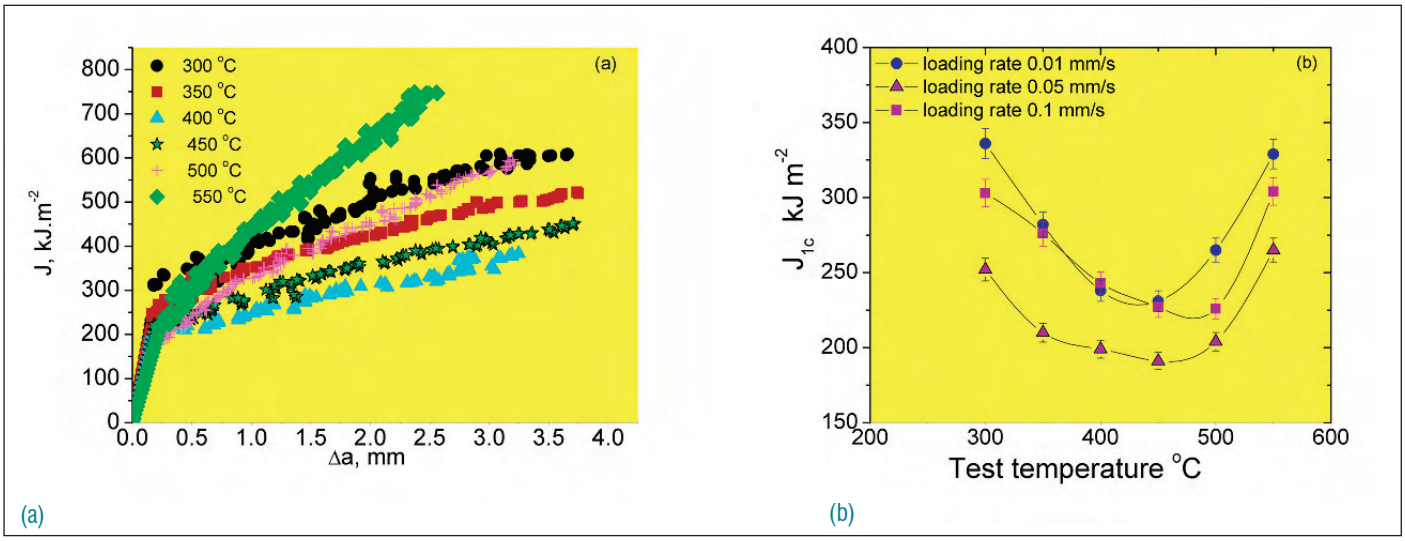

Figure 3 (a-b) : Fracture properties of the steel (a) J-R curves and (b) average fracture toughness values

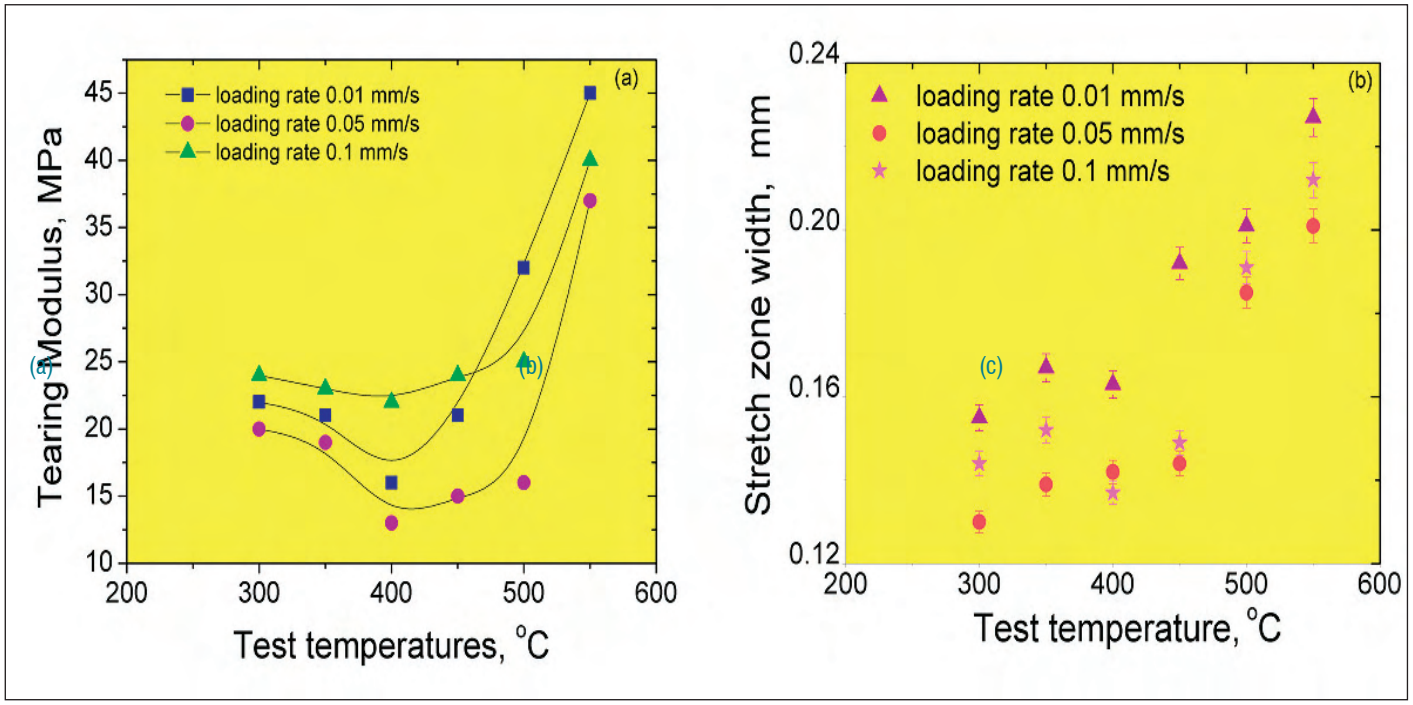

Figure 4 (a-b) : Fracture properties of the steel (a) Tearing Modulus and (b) average stretch zone width values

no.2) was derived for plane strain condition. The n values (Figure 2) varied between 0.29 and 0.38 for various temperatures. For equation 2, h3(a/w,n) is geometry dependent function. For CT specimen having crack length to width ratio of 0.6, an approximate value of h3 =1.8 was considered for this function. The estimated (Figure 5) crack tip strain rates varied between 10-3 and 10-4 s-1.

The estimated strain rates were considered based on minimum

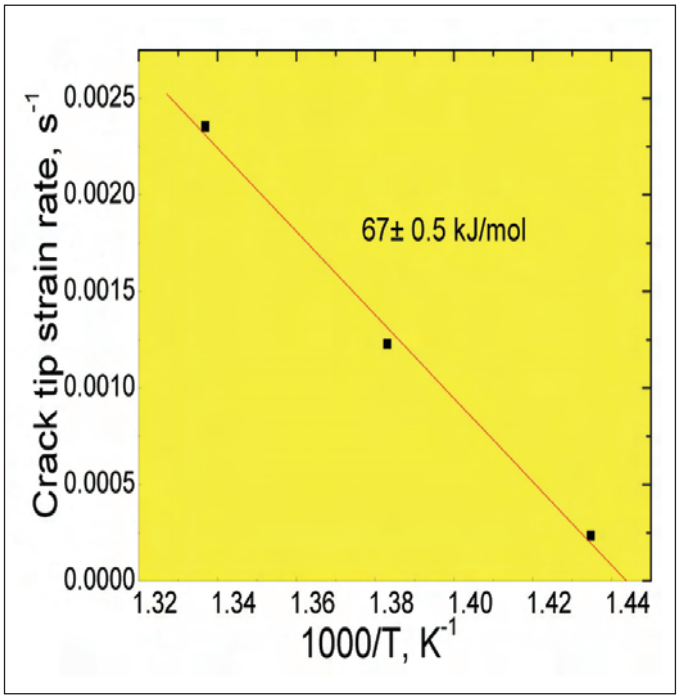

Figure 5: plots of estimated crack tip strain rates

values of fracture toughness in the temperature range 400- 475 °C and plotted as shown in Figure 5. The activation energy was ~ 67±1 kJ/mol. The activation energies for this class of steels were previously reported in the range 55-80 kJ/mol. Generally, this activation energy value range (55-80) corresponded to the energy for diffusion of interstitial atoms. Thus, it can be stated that the dynamic interaction between moving dislocations and interstitial solute (C, N) are responsible for DSA. The above results can be summarized as follows. The fracture behavior of Grade 91 steel has been examined in the temperature range 300-550 °C and found to be minimum at intermediate temperature range. This is attributed to the DSA. The dynamic interaction between moving dislocations and interstitial solute (C, N) atoms are responsible for DSA. These observations were supported by the tensile properties.

The above mentioned fracture toughness data (Figure 3b) can be used as input towards determination of structural integrity of the SG components. The J-R curves (Figure 3a) and tearing modulus values (Figure 4a) are also used to evaluate tearing resistance of these SG components of various geometries and under different loading conditions. A detailed analysis to evaluate tearing resistance and structural integrity assessment, based on material properties and the relevant design guidelines may not be included in this report. From a preliminary assessment of the above mentioned fracture data, it can also be inferred that under operating temperatures the susceptibility of this material towards brittle failure is negligible.

Young Researcher's FORUM

2D-V_2O_5 Nanosheets for Photocatalytic and Advanced Energy Storage Applications

Reshma P R received her Bachelor of Science (B.Sc) and Master of Science (M.Sc) in Physics from Sree Krishna College Guruvayoor, University of Calicut in 2013 and 2015 respectively. She joined IGCAR as research fellow in August 2016 under Homi Bhabha National Institute, IGCAR, Kalpakkam, India. Currently she is pursuing her doctoral studies in the area of synthesis, characterization and applications of 2-D metal oxide nanostructures.

2D materials are known for their exotic physical, chemical, and electronic properties which are markedly different from the bulk form. The properties of these materials can be tuned with the number of layers. This creates scope for tuning electronic, optical, magnetic, and surface properties for various applications. 2D transition metal oxides (TMO) stand out from other 2D materials due to their capability of existing in different binding configurations. But, unlike other 2D materials, 2D TMOs are difficult to synthesize because of the surface structural reconstruction which compensates for the instability in 2D form. In the present study the 2D-V_2O_5 nanosheets are synthesized and used for catalysis and energy storage applications.

Photocatalytic Applications

In the present study, 2D-V_2O_5 nanosheets were synthesized using the chemical exfoliation technique by optimizing the concentration of bulk V_2O_5 in formamide. The suspension of exfoliated 2D-V_2O_5 flakes in formamide was directly drop coated on SiO_2/Si substrate and high pure Au substrate and heated at 100°C for removing remnants of formamide. Post annealing treatment was performed at 250 °C for 3 h in O_2 atmosphere. Figure 1a shows the schematic of the exfoliation process. Figure 1b shows the sample dispersion. The atomic force microscopic (AFM) image in figure 1c shows that the thickness of the layers is in the range of 1- 1.5 nm, equivalent

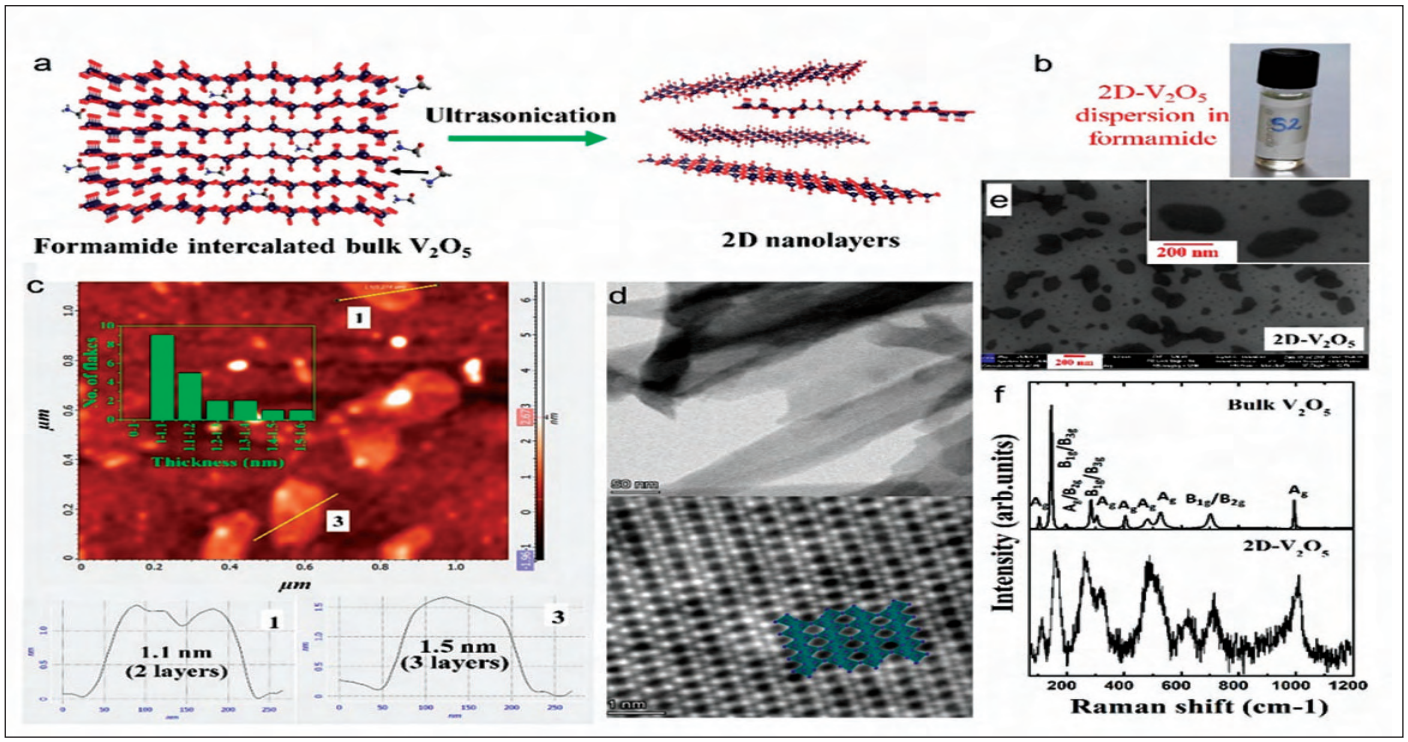

Figure 1: a) Schematic diagram showing the exfoliation of α-V_2O_5 using formamide as the intercalating agent. b) The picture of 2D-V_2O_5 nanosheet dispersion in formamide. c) AFM image and the step height of nanosheets in the image. The number distribution of thickness of nanosheets are showed in the inset of the Figure. d) Bright-field STEM image of V_2O_5 nanosheets and atomic resolution iDPC-STEM image of the bilayer thin nanosheet of V_2O_5. e) FESEM image of 2D-V_2O_5. The inset shows magnified views of the respective images. f) The Raman spectra of bulk and 2D-V_2O_5.

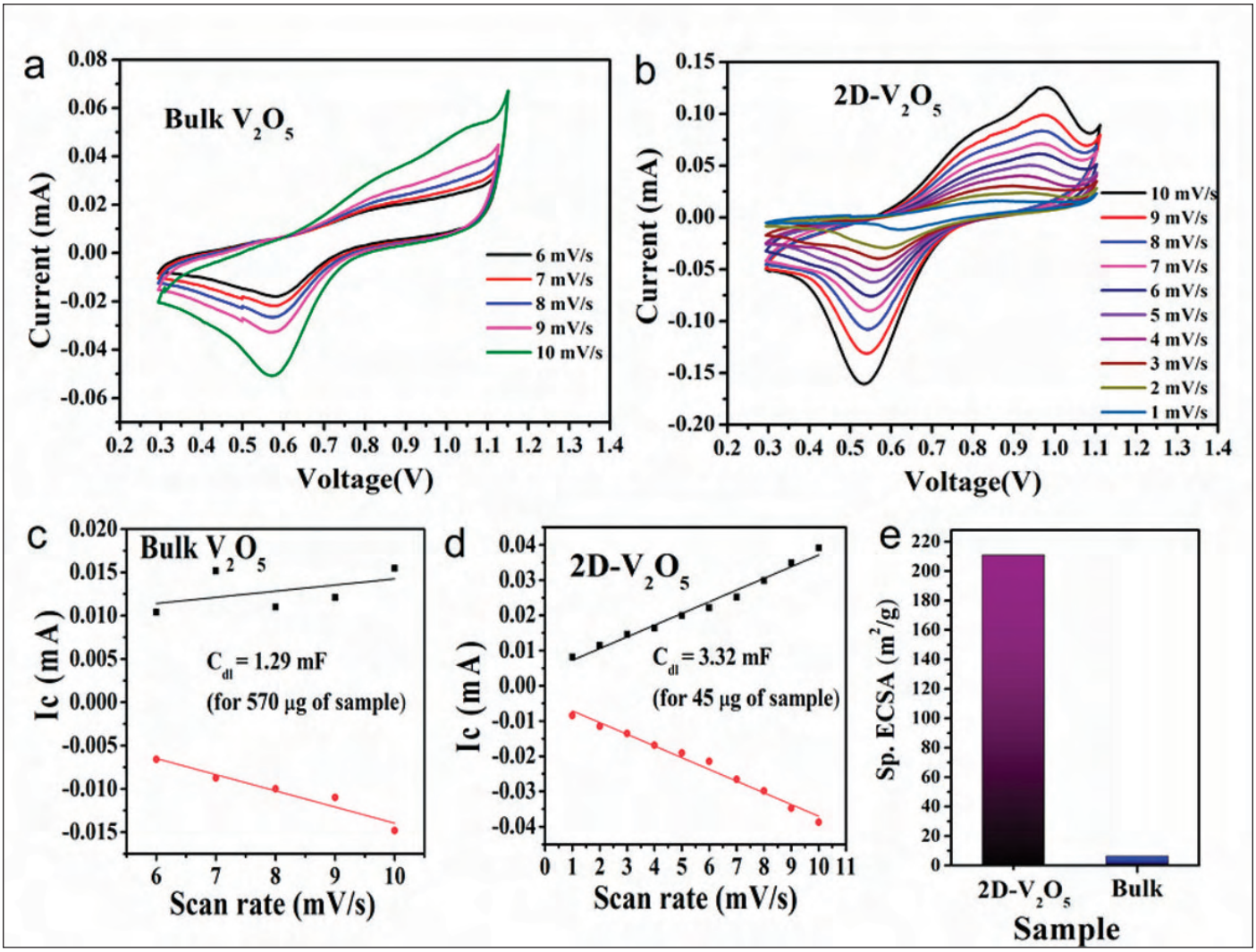

Figure 2: CV diagram of a) bulk V_2O_5, b) 2D-V_2O_5. The curve of the peak current with scan rate in the non-Faradic region for c) bulk V_2O_5, d) 2D-V_2O_5. The value of double layer capacitance (Cdl) is given in the inset. g) ECSA for 1g of bulk V_2O_5 and 2D-V_2O_5.

to two to three layers of V_2O_5. The atomic resolution transmission electron microscopic image (Figure 1d) shows that the phase of the exfoliated bilayer nanosheets is retained after exfoliation. Field emission scanning electron microscope (FESEM) images of the sample is shown in Figure 1e. The Raman spectrum collected from the 2D-V_2O_5 also substantiates the formation of bilayer structure according to an earlier study carried out by our group (Figure 1f).

In order to understand the surface activity of 2D-V_2O_5, the specific surface area of the exfoliated V_2O_5 nanosheets are compared with that of the bulk V_2O_5 by calculating the electrochemically active surface area (ECSA). In the present study, cyclic voltammogram (CV diagram) of the samples (figure 2a and 2b) with 1M H_2SO_4 electrolyte are recorded and the peak current, Ic is taken from the non-Faradic region. The experiment is carried out in a three electrode set up with Pt electrode as the counter electrode and Ag/AgCl as the reference electrode. Each hydrogen atom from the electrolyte is assumed to get adsorbed onto every atom on the sample surface. Hence, the ECSA can be calculated as, ECSA= Cdl/Cs, Where Cs is the specific capacitance of an atomically smooth planar surface of the material per unit area under identical electrolyte conditions and Cdl is the double layer capacitance of the sample. For 1M H_2SO_4 electrolyte, the value of Cs is 0.035 mF/cm^2.

In the present study, bulk V_2O_5 sample was prepared by coating 630 μL of 5 mM dispersion of bulk V_2O_5 in propanol on carbon paper of dimension 1.5cm × 1.5cm. Hence 570 μg of the sample was coated on the substrate. While for 2D V_2O_5, 250 μL of 1 mM dispersion of exfoliated V_2O_5 nanosheets in formamide is coated uniformly on carbon paper of 1.5 cm × 1.5 cm dimensions. Hence, 45 μg of sample was used for the measurement. The CV diagram of bulk and 2D V_2O_5 are given in figures 2a and 2b respectively. The value double layer capacitance (Cdl) is found to be 1.29 mF and 3.32 mF for bulk and 2D V_2O_5 respectively (Figure 2c and 2d). The corresponding ECSA per 1 g of the samples are found to be 6.5 and 211 m^2/g for bulk and 2D V_2O_5 respectively (Figure 2e). The bulk V_2O_5 is reported to be a material with very low specific surface area typically less than 10 m^2/g. The observed value of the specific

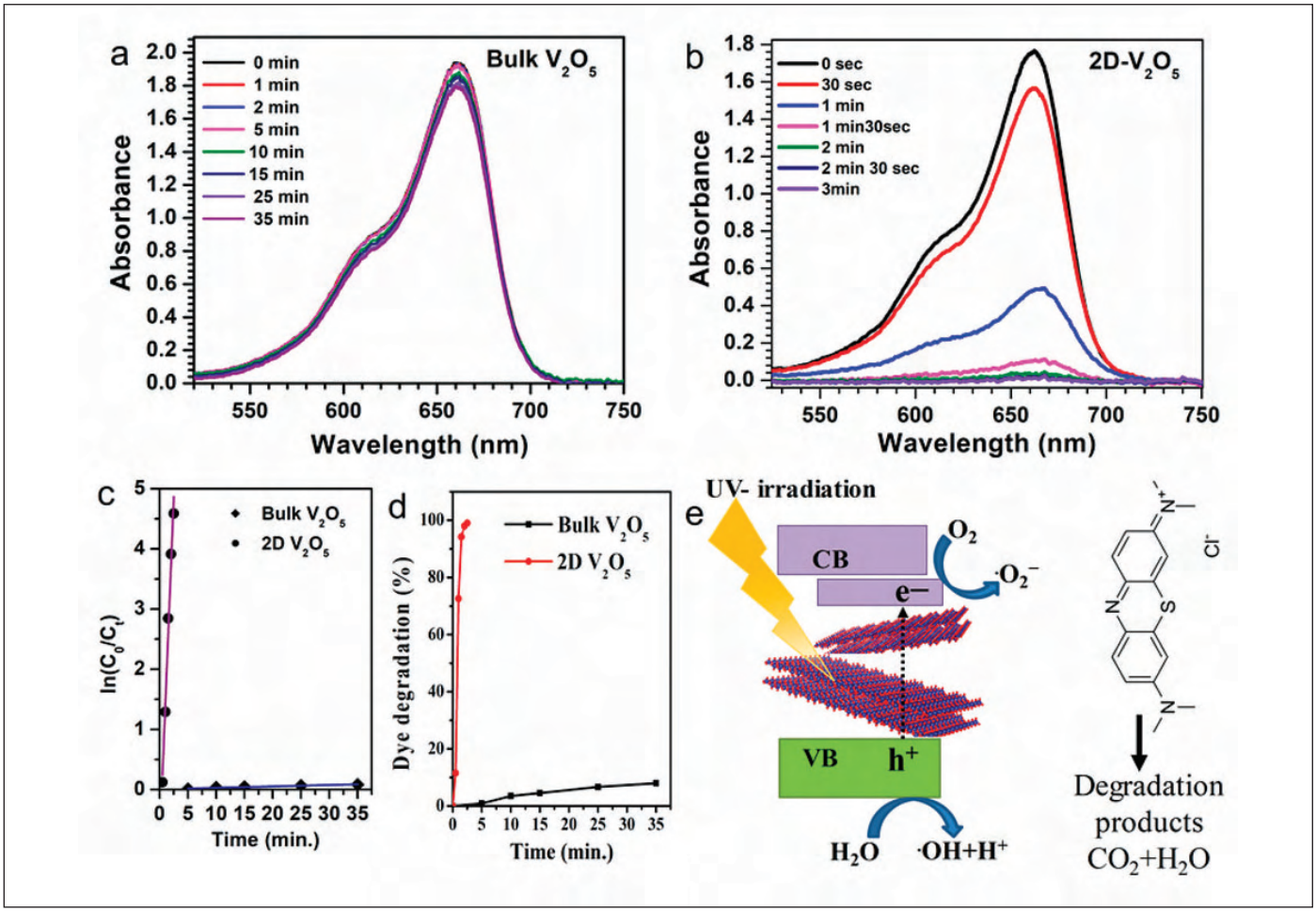

Figure 3: The UV-Vis absorption spectra of methylene blue (MB) dye solution with different light exposure time in the presence of a) bulk V_2O_5 and b) 2D-V_2O_5 as catalysts. c) the curve of $\ln(C_0/C_t)$ v/s light exposure time, for finding the rate constant of dye degradation using bulk and 2D-V_2O_5 catalysts. d) curve showing the dye degradation percentage (efficiency) using bulk and 2D V_2O_5 catalysts with time of light exposure. e) schematic diagram showing the dye degradation mechanism by 2D V_2O_5.

surface area is thus consistent with the literature values. Hence, a ~32 times increase of specific surface area is observed for 2D V_2O_5 in comparison to its bulk counterpart.

The large increase in the surface to volume ratio can enhance the catalytic property of 2D-V_2O_5. In order to examine the photocatalytic properties of bulk and 2D V_2O_5, degradation of Methylene blue (MB, $C_{16}H_{18}ClN_3S$ (Merck India)) dye is examined. V_2O_5 catalyst was used to degrade the dye under UV-C. Aqueous solution of dye and bulk V_2O_5 catalyst (concentration of 0.18 mg/ml of catalyst) was made in the dark and kept for adsorption-desorption equilibrium. For 2D-V_2O_5, 0.9 mg of sample (5 ml of 1 mM sample dispersion in formamide) is coated on quartz substrate by dipping into 5 ml of dye solution. It is kept in dark for adsorption-desorption equilibrium. Then the dye solution with the catalyst was exposed to the light source for different intervals of time and 3 ml of the irradiated solution was analyzed using a UV-Visible spectrometer. Degradation of MB was monitored by recording the absorption peak of MB at 664 nm. Periodically, UV-Vis absorption spectra of the solutions were recorded for quantitative analysis. Figure 3a and b show the UV-vis absorption spectra of aqueous dye solution with bulk 2D V_2O_5 catalysts, taken in particular time intervals of UV light exposure. The reduction in the intensity of absorption peaks at 662 and 608 nm shows breakage of the benzene ring and heteropoly aromatic linkage of MB dye molecule. Hence, in the presence of the catalyst under the exposure with UV radiation, the dye molecules undergo degradation. As it is observed from the figure 3a, the bulk V_2O_5 catalyst caused degradation of 16 ppm dye up to a very small extent with a UV exposure of 35 min. Whereas, 2D-V_2O_5 catalyst degraded ~ 99% of the 16 ppm dye with an UV exposure of 3 min.

The degradation reaction is observed to follow the pseudo-first order kinetics and fits well with the equation, $\ln\frac{C_0}{C_t} = kt$, where C_0 is the initial absorption of the dye and C_t is the absorption after the time interval, t for the light irradiation (Figure 3c). The rate constant k represents the quickness of the degradation process. The rate constant for the dye degradation by bulk and exfoliated V_2O_5 catalyst were evaluated from the Figure 3c. The rate constant of MB dye degradation by bulk and 2D-V_2O_5 catalysts are 0.0023 and 2.311 m^{-1} respectively. The photocatalytic dye degradation efficiency in

percentage (%) was calculated using the equation, $D(\%) = \frac{C_0 - C_t}{C_0} \times 100$. In the presence of bulk V_2O_5 catalyst, 7.7% dye degradation is observed in 35 min of light exposure. While, in the presence of 2D-V_2O_5 catalyst, ~99% of the dye degraded under 3 min of light exposure. The figure 3d shows the change in degradation efficiency with three catalysts with light exposure time. The MB dye molecule contain active sites for oxidative attack. The possible mechanism of catalysis is as shown in the Figure 3e. Under UV light irradiation, the electrons are excited to the conduction band (CB) of V_2O_5, leaving holes behind in the valence band (VB). These holes will react with OH^- on the surface of the catalyst to form •OH radicals. The electrons accepted by V^{5+} ions are transferred quickly to oxygen molecules under the surrounding conditions to regenerate V^{4+} to produce $\bullet O^-_2$ superoxide anion radicals. The •OH and $\bullet O^-_2$ radicals are the oxidizing species in the photocatalysis reaction. These results suggest that the separation of electrons and holes can effectively be enhanced by 2D V_2O_5 nanosheets, which will greatly enhance the photocatalytic activity compared to the earlier reports as showed in the table 1

Table 1: Comparison of the present results with the reported literature

Photocatalyst	Rate constant min−1	Degradation time (m)	Efficiency (%)
V_2O_5-np	0.00742	20	31
rGO-V_2O_5	0.0184	20	71
V_2O_5-nanorods	0.00135	300	24
Graphene- V_2O_5	0.0367	90	98
Nd3+ doped V_2O_5	--	120	80
2D-V_2O_5	2.311	3	~99

Advanced Energy Storage Applications

The increased consumption of energy demands the development of new energy storage facilities. The idea of employing hybrid ion batteries originated recently to provide improved ion-intercalation battery performance. V_2O_5 is widely used as a cathode material for ion intercalation battery, because of its layered structure, low toxicity, ease of synthesis, and availability. But, its 2D counterpart is not well studied for the application. Hence, the use of 2D-V_2O_5 nanosheets in Zn-Li hybrid battery is explored.

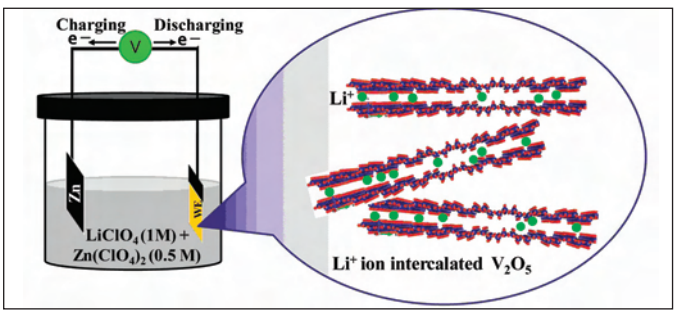

Figure 4: The schematic diagram of the battery set-up

The battery performance is tested at room temperature, using a commercial potentiostat (PGSTAT 302N, Metrohm Autolab e.v.). The electrochemical cell was prepared with Zn metal as the counter electrode. The working electrode was prepared by depositing the exfoliated V_2O_5 nanosheets on carbon paper. 4.8 ml of sample dispersion solution (1 mM) was coated on the carbon paper with a length of 2 cm and a breadth of 1.5 cm. As a result, 0.864 mg of 2D-V_2O_5 nanosheet sample was loaded on the carbon paper. The cyclic voltammogram (CV) and charging-discharging were carried out from 0 to 2.8 V (V vs Zn electrode). The schematic diagram of the experimental set-up is shown in the Figure 4.

The cyclic voltammogram (CV) collected from the sample at 10 mV/sec is shown in figure 5a. The CV exhibited three reduction peaks at 0.6, 0.9 and 1.2V. The oxidation peaks were observed at 0.56, 1.1, 1.4, and 2.4. The peaks arise due to the intercalation and de-intercalation of Li^+ ion into the V_2O_5 nanosheets. During the intercalation (discharging of the battery) of Li+ ions into the crystal, the V^{5+} atoms in the crystal undergoes reduction to V^{3+} (for number of charges involved in the intercalation/de-intercalation process, z=4) or V^{4+} (for, z=2). During the de-intercalation (charging) the reduced V^{3+} or V^{4+} ions undergo oxidation to V^{5+}. Hence the half-cell reactions during charging and discharging can be represented as,

For discharging, $xZn \rightarrow xZn^{2+} + 2x\ e^-$ (Anode reaction)

$V_2O_5 + 2x\ Li^+ + 2x\ e^- \rightarrow Li_{2x}V^{((5-x)+)}{}_2O_5$ (Cathode reaction)

And for charging , $Li_{2x}V^{((5-x)+)}{}_2O_5 \rightarrow V_2O_5 + 2x\ Li^+ + 2x\ e^-$ (Cathode reaction) $x\ Zn^{2+} + 2x$ e- → x Zn (Anode reaction)

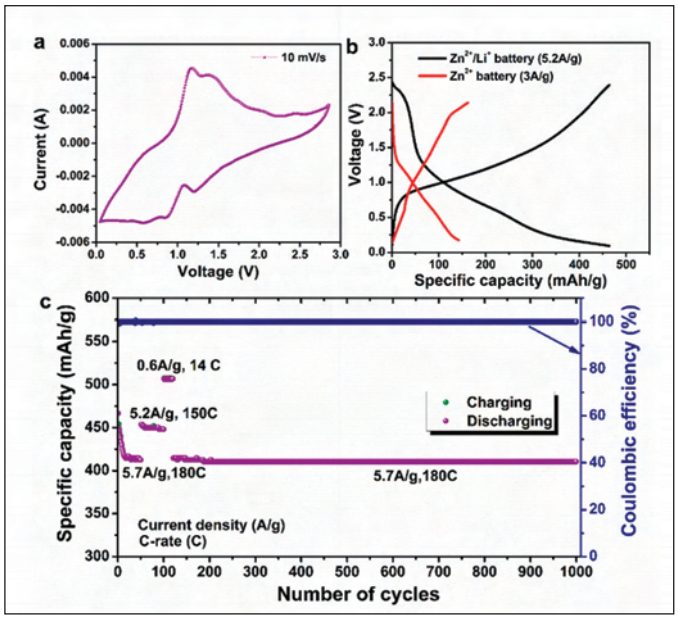

Figure 5: a) Cyclic voltammogram of hybrid ion battery set up. b) comparison of charge-discharge profile of Li/Zn hybrid ion battery with Zn ion battery. c) The specific charge capacity and coulomb efficiency of Li/Zn hybrid ion battery

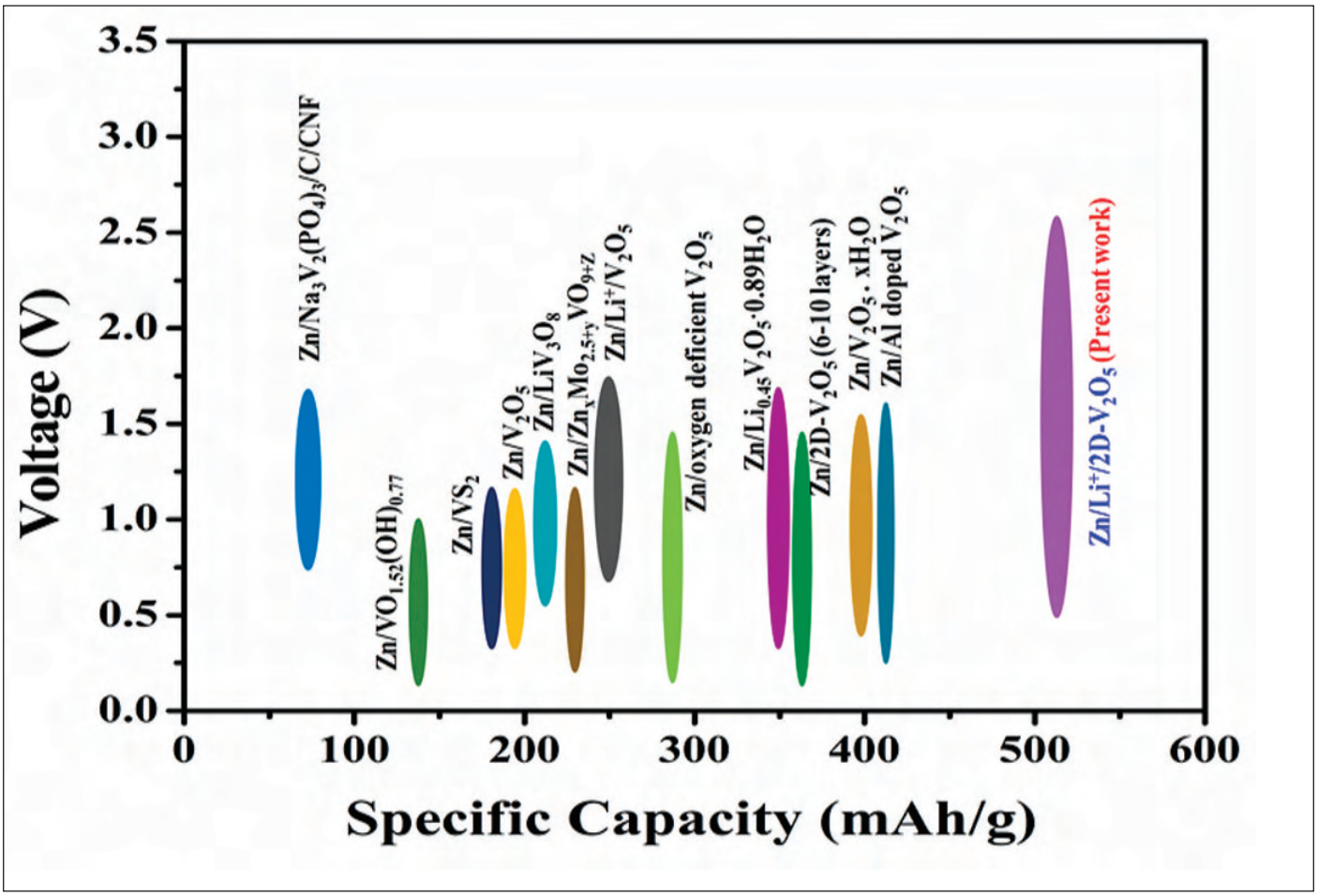

Figure 6: The comparison of the present results with the literature.

The charge/discharge profile for zinc ion battery (ZIB) and Li intercalated ZIB (ZLIB) shown in figure 5b, indicates that the battery performance is improved in ZLIB than ZIB. The specific charge capacity of the battery is calculated using the equation, $Q = It/m$, where I, t, and m are charging/discharging current, charging/discharging time, and mass of active material respectively. Figure 5b shows that the specific charge capacity of ZLIB showed approximately two-fold increase from ZIB along with the increase in operating voltage. The increase in operating voltage for ZLIB offers a higher power density associated with the battery. The specific charge capacity and coulombic efficiency of the battery with the number charge/discharge cycles are shown in figure 5c. The columbic efficiency (η) of a battery is the ratio of the discharging specific capacity with the charging specific capacity. The parameter quantitatively shows the number Li^+ ions which stays inside the active material during de-intercalation. The specific charge capacity of the battery is calculated as 410.5 mAh/g, 450 mAh, and 510 mAh/g with the current densities 5.7A/g, 5.2 A/g, and 0.6 A/g respectively. The value of specific capacity of the battery with a fast charging current density of 0.6 mAh/g stands out from the vanadium oxide based ZIB as shown in figure 6. The present results are compared with the specific capacities from previous studies with similar current densities (an indicative of the charging/discharging rate). The battery showed a coulombic efficiency of $\sim$ 99% from the first cycle till the 1000 cycle. This high coulombic efficiency of the battery derives from the diffusion property of Li^+. Hence the use of hybrid ion battery improves not only the specific charge capacity of the battery, but also the coulombic efficiency and cyclic performance.

The present findings show that 2D-V_2O_5 nanosheets exhibits exceptional battery performance as indicated in the figure 6. The reason for the improved battery performance originates from the cathode material property. The 2D-V_2O_5 nanosheets used as the cathode material contain bilayer and trilayer nanosheets. The thickness of the nanosheets is in the range of 1.0-1.5 nm. According to the definition of the monolayer V_2O_5, the thickness of synthesized nanosheets are larger than the theoretical thickness. The increase in thickness of synthesized nanosheets indicate an increase in the interlayer separation. As a result, the sample provides an easier pathway for the ion diffusion. The use of hybrid ion battery also helped in improving the performance. The increase in battery performance is associated with the availability of Li^+ ions for intercalation.

One-day Workshop on Intellectual Property Rights

April 26, 2022

Inaugural Session of the workshop in progress

A one-day Workshop on Intellectual Property Rights was jointly organised by Incubation Centre-IGCAR, Kalpakkam and Intellectual Property Rights Cell, DAE Mumbai with support from Administrative Training Institute, DAE (program code: 19) on 26th April 2022. The objective of the workshop was to create awareness amongst IGCAR scientists and engineers on the importance of protecting their intellectual property rights and transforming lab based ideas into commercially viable technologies through incubation and technology transfer routes. Considering the theme of the workshop and the fact that 26th of April each year is celebrated internationally as World Intellectual Property Day with the focus on youth and IP this year, nominations were invited from young officers and technical staff of various R&D groups of IGCAR as well as other Kalpakkam based DAE Units such as BARCF (including NRB & FRFCF) and GSO. A total of 83 nominations were received from IGCAR groups, BARCF and GSO.

The workshop started with a welcome note by Dr .N. Subramanian, Head, Incubation Centre-IGCAR, followed by introduction of the workshop faculty. Shri Dani Rajiah Member Secretary, IPR Cell, DAE briefly explained the objectives of the workshop.

Guest Speaker, Lawyer Ms. Anuradha Maheshwari, delivering her lecture at the workshop

Smt Anuradha Maheswari, Ex-director, Institute of Intellectual Property Studies and Partner, Lex Mantis Advocates, Mumbai was the Guest Speaker at the workshop. In a marathon session of three lectures, she explained in detail about nature and types of IPR, history of IPR, timelines, criteria and procedures of patenting, non-patentable inventions, etc. She also talked about PCT filing and international patents. In the final lecture, she dwelt upon the importance of valuation of technology and commercialization.

Next Dr. N. Subramanian, Head, IC-IGCAR explained about functioning of the DAE Incubation Centre at IGCAR, the TRL guidance chart and the mechanisms available for DAE researchers to transform innovative ideas into commercializable technologies through incubation route.

Shri Daniel Babu, Technology Transfer and Collaborations Division, BARC, Mumbai explained in detail about the extant technology transfer mechanism in BARC. He emphasized on opening up of new links between research institutions and industry.

Shri Dani Rajiah gave a informative lecture highlighting DAE experiences with patenting. He gave a clear take-home message to the participants that sincere efforts should be taken to commercialize their patents. Feedback received from all the participants was excellent and they felt it was a fantastic exposure for them on IPR, incubation and technology transfer mechanisms. The workshop concluded with a vote of thanks proposed by Dr.Anita Toppo, Member, IC-IGCAR, Kalpakkam.

Reported by

Dr .N. Subramanian, Head, Incubation Centre-IGCAR,

2nd Foundation Day of Indira Gandhi Centre for Atomic Research, Kalpakkam

April 30, 2022

Shri G. Nageswara Rao, Chairman, AERB releasing the booklet "Journey of FBTR - Reaching Further Heights" during the 2nd Foundation Day of IGCAR along with Shri S. Raghupathy, Director, RDTG & EIG, Dr. Shankar V. Nakhe, Director, RRCAT, Dr. B. Venkatraman, Director, IGCAR Dr. P. R. Vasudeva Rao, Vice Chancellor,HBNI, Dr. D. K. Sinha, Director, AMD, K. R. Sethuraman, CAO, IGCAR

Organizational set up for Reactor Research Centre, now renamed as Indira Gandhi Centre for Atomic Research (IGCAR), was approved by Dr. Vikram Sarabhai, the then Secretary, DAE, & Chairman, Atomic Energy Commission, on 30th April 1971. Foundation Day is an important occasion to reflect on the beginning of the Organization, recalling the fond memories, the wisdom, courage, commitment, the enormous challenges faced by our seniors and the significant scientific and technological contributions made by them in developing indigenous technologies, the privilege we had of sharing their expertise and work ethics even while expressing our gratitude to them.

Indira Gandhi Centre for Atomic Research celebrated its 2nd Foundation day on 30th April 2022 with great fervour. This year was very significant because our Organization completed 51 years since its inception, 50 years after the first ground breaking of our flagship Fast Breeder Test Reactor, which also attained its designed capacity of 40 MWt on 07th March 2022.

Shri G. Nageswara Rao, Chairman, Atomic Energy Regulatory Board, Mumbai, Dr. P. R. Vasudeva Rao, Vice Chancellor, Homi Bhabha National Institute, Mumbai, Dr. D. K. Sinha, Director, Atomic Minerals Directorate for Exploration and Research, Hyderabad, Dr. Shankar V. Nakhe, Director, Raja Ramanna Centre for Advanced Technology, Indore, were our Guests of Honour, on this grand occasion.

Programme Highlights

Shri S. Raghupathy, Director, Reactor Design & Technology Group and Electronics & Instrumentation Group, IGCAR, delivered the Welcome Address. Dr. B. Venkatraman, Director, IGCAR, made a presentation on the activities of IGCAR. Dr. D. K. Sinha, Director, AMD, delivered a talk on the exploration activities and the contributions of AMD to the Nuclear Power Programme. Dr. Sinha released a Hindi booklet titled "द्रुत रिएक्टर प्रौद्योगिकी के क्षेत्र में 51 वर्षों की यात्रा: एक झलक".

Dr. P. R. Vasudeva Rao, Vice Chancellor, HBNI, delivered a talk on the importance of metallic fuel for the future of the nuclear power programme. Dr. Vasudeva Rao distributed the awards for best Ph.D./M.Sc. (Engg.)/M.Tech thesis nominations for the last three years. Dr. Shankar V. Nakhe, Director, RRCAT, delivered a talk on the Laser and Electron Beam technologies and its societal benefits. Dr. Shankar V. Nakhe released a book titled "Butterflies of Kalpakkam" and distributed Certificate of Appreciation for Ph.D./M.Sc. (Engg.)/M.Tech thesis. Shri G. Nageswara Rao, Chairman, AERB, delivered a talk on the role of regulatory authorities and the use of radiation technologies for societal benefits. Shri Nageswara Rao inaugurated the "Integrated Radiation Monitoring Facility" building at Anupuram Township and remotely inaugurated "Chopping of Uranium Oxide pins at Demonstration Fuel Reprocessing Plant". Shri Nageswara also released a document titled "Journey of FBTR - Reaching Further Heights". Views, thoughts and opinions expressed by the distinguished dignitaries radiated a source of energy and set a perfect platform for the occasion. Shri K. R. Sethuraman, Chief Administrative Officer, proposed the vote of thanks.

Reported by
K. R. Sethuraman Chief Administrative Officer, IGCAR

Inauguration of Integrated Radiation Monitoring Facility

April 30, 2022

Shri. G. Nageswara Rao, Chairman, AERB, along with Dr. B. Venkatraman, Director, IGCAR and senior colleague while Inaugurating IRMF building at Anupuram

Integrated radiation monitoring facility consisting of in-vivo & in-vitro monitoring laboratories and a decontamination centre, meeting the latest NDMA and AERB guidelines is established at Anupuram hospital complex. The facility is designed to cater to the entire Kalpakkam complex to provide monitoring service both under normal as well as radiological emergency conditions. The facility was inaugurated by Shri. G. Nageswara Rao, Chairman, Atomic Energy Regulatory Board on April 30, 2022.

Integrated Radiation Monitoring Facility building at Anupuram

Reported by

Dr. D. Ponraju, AD, HSEG & Head, HISD

HBNI-IGCAR CI

Ph.D Thesis Defense

Name	Title	Discipline
Pamarthi Amesh	Development of organo-functionalized high capacity adsorbents for the recovery of uranium from aqueous solution and seawater	Chemical Sciences
Deepitha J	Solubility studies on ligands in supercritical carbon dioxide medium and its application to extraction of some heavy metal ions	Chemical Sciences
Dr. Arjun Pradeep	Mass Transfer from Rising Mixed Gas Bubble in Quiescent Liquid Pool of SFR	Engineering

Certificate of Appreciation

Name	Title	Discipline
Shri. Padmalochan Panda.	Synthesis and Characterization of Pristine and Doped (Ti and Cr) AlN Thin Films	Physical Sciences
Shri. Sithara Vinod	Studies on the effect of magnetic field induced aggregation on physical properties of ferrofluids	Physical Sciences
Shri Binaya Kumar Sahu	Growth and Applications of Low Dimensional SnO_2	Physical Sciences

Awards, Honours and Recognitions

Dr. B.Venkataraman and Dr. John Philip have been conferred the Honorary Fellowships of the Indian Society of Analytical Scientists, Mumbai.

Dr. John Philip has been appointed as Associate Editor of Frontiers in Nanotechnology (Nanomaterials), Frontiers Publishing, UK

Dr. John Philip has been selected as an Editorial board member of Smart Materials in Medicine, Elsevier, Netherland

Dr. John Philip has been selected as an Editorial board member, Materials Futures, Institute of Physics(IOP), UK

Best Paper Award

K.K. Madapu, C. Abinash Bhuyan, S. K. Srivastava, S. Dhara
The novel mechanism in understanding a strong enhancement of photoluminescence quantum yield in large-area monolayer MoS_2 grown by CVD. J. Mater. Chem. C 9 (2021) 3578

Bio-diversity @ DAE Campus, Kalpakkam

Little Grebes are aquatic birds adapted for diving in from the surface and swimming under the water. Grebes are migratory birds found in WIP marsh area. Normally sedentary, but capable of flying long distances during drought to find new habitats.

Published by Scientific Information Resource Division, SQ&RMG, IGCAR, Kalpakkam-603102